The Astrophysical Journal, 685:261–271, 2008 September 20

IDENTIFYING STELLAR STREAMS IN THE FIRST RAVE PUBLIC DATA RELEASE

R. Klement,[1] B. Fuchs,[2] and H.-W. Rix[1]
Received 2007 August 7; accepted 2008 May 15

ABSTRACT

We have searched for and detected stellar streams or moving groups in the solar neighborhood, using the data provided by the first RAVE public data release. This analysis is based on distances to RAVE stars estimated from a color-magnitude relation calibrated on *Hipparcos* stars. Our final sample consists of 7015 stars selected to be within 500 pc of the Sun and to have distance errors better than 25%. Together with radial velocities from RAVE and proper motions from various databases, there are estimates for all six phase-space coordinates of the stars in the sample. We characterize the orbits of these stars through suitable proxies for their angular momentum and eccentricity and compare the observed distribution with the expectations from a smooth distribution. We identify at least four "phase-space overdensities" of stars on very similar orbits in the solar neighborhood. We estimate the statistical significance of these overdensities by Monte Carlo simulations. Three have been identified previously: the Sirius and Hercules moving groups and a stream found independently in 2006 by Arifyanto & Fuchs and Helmi et al. In addition, we find a new stream candidate on a quite radial orbit, suggesting an origin external to the Milky Way's disk. Also, there is evidence for the Arcturus stream and the Hyades-Pleiades moving group in the sample. The detections are further supported by analyzing the stellar distribution in velocity and angular momentum space using the Monte Carlo simulations. We find that the significance of overdensities is comparable, independent of the space in which the stream search is conducted. This analysis, using only a minute fraction of the final RAVE data set, shows the power of this experiment to probe the phase-space substructure of stars around the Sun.

Subject headings: Galaxy: kinematics and dynamics — solar neighborhood

1. INTRODUCTION

According to current ideas about the cosmogony of galaxies, they assembled through hierarchical merging, which should result in a richly structured phase-space distribution of dark matter and stars. Direct empirical evidence for such events has been sought among the stellar populations of the Milky Way with large-scale surveys. Ongoing satellite accretion events have been discovered in several instances. A prominent example is the Sagittarius galaxy (Ibata et al. 1994) with its associated tidal stream, which wraps around the Galaxy nearly perpendicular to the Galactic plane (Ibata et al. 2001; Majewski et al. 2003; Belokurov et al. 2006). Similarly, the Monoceros stream at low Galactic latitudes (Yanny et al. 2003; Ibata et al. 2003) and the recently discovered Orphan stream (Belokurov et al. 2006) are interpreted as tidal debris from the Canis Major and Ursa Major II dwarf galaxies, respectively (Peñarrubia et al. 2005; Fellhauer et al. 2007). Numerical simulations have shown that such debris streams can survive as coherent structures for gigayears (Helmi et al. 2003; Peñarrubia et al. 2005; Law et al. 2005).

Star streams, that is, groups of stars on essentially the same orbits in the Galactic potential, have also been detected as overdensities in the phase-space distribution of stars in the solar neighborhood. The concept of "moving groups" originates from the work of Olin Eggen (Eggen 1996 and references therein). Some of the moving groups are associated with young open clusters and can be naturally explained as clouds of former members, now unbound and drifting away from the clusters; these moving groups only reflect the nature of star formation, not necessarily that of hierarchical galaxy formation.

However, data from the last decade seem to support the concept of cold star streams in the solar neighborhood, consisting of old stars (5–10 Gyr). Helmi et al. (1999) discovered the signature of a cold stream in the velocity distribution of halo stars, which had been constructed from *Hipparcos* data. This was later confirmed by Chiba & Beers (2000) using their own data. Helmi et al. (1999) argued that this stream forms part of the tidal debris of a disrupted satellite galaxy accreted by the Milky Way, which ended up in the halo. Moreover, Navarro et al. (2004) interpreted Eggen's Arcturus stream as another such debris stream, but in the thick disk of the Milky Way, dating back to an accretion event 5 to 8 Gyr ago.

Moving groups of old stars are also observed in the velocity distribution of thin-disk stars in the solar vicinity. Based on *Hipparcos* parallaxes and proper motions, Dehnen (1998) found with statistical methods new evidence for the Sirius-UMa, Hyades-Pleiades, and Hercules star streams. Even more convincingly, these streams show up in the three-dimensional kinematic data for F and G stars in the Geneva-Copenhagen Survey (Nordström et al. 2004). These moving groups are very probably not related to tidal debris streams but originate from dynamical effects within the disk itself, such as resonances with the inner bar of the Milky Way (Dehnen 2000) or with spiral density waves (Quillen & Minchev 2005).

Yet another stream has been discovered independently by Arifyanto & Fuchs (2006) and Helmi et al. (2006), analyzing different data samples and applying different detection techniques. The metallicities of the stars in this stream cover a broad range, from those typical for old thin-disk stars to that of thick-disk stars. Thus, the exact nature of this stream seems to be at present not fully understood.

With the first data release (DR1) from the Radial Velocity Experiment (RAVE; Steinmetz et al. 2006), a large new data sample of stars in the Milky Way became available, which is ideally suited for kinematic studies. To explore RAVE's potential, we analyze the velocity distribution of more than 7000 stars within a distance

[1] Max-Planck-Institut für Astronomie, D-69117 Heidelberg, Germany; klement@mpia.de, rix@mpia.de.
[2] Astronomisches Rechen-Institut am Zentrum für Astronomie Heidelberg, D-69120 Heidelberg, Germany; fuchs@ari.uni-heidelberg.de.

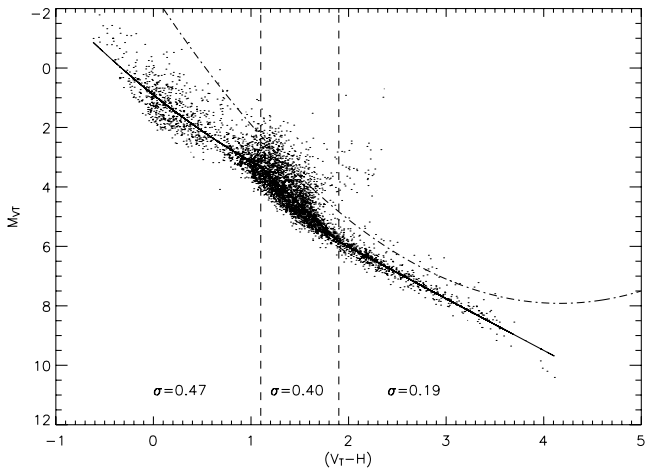

FIG. 1.—Absolute magnitude calibration for *Hipparcos* MS stars with a parallax accuracy better than 10% with V_T-H as the color. All stars above the dash-dotted line are assumed to be giants incorrectly classified as MS stars and are not considered for the color-magnitude fit. The solid line shows the M_{V_T}-(V_T-H) relation adopted, and the dispersions σ about this mean relation are indicated in three color regimes.

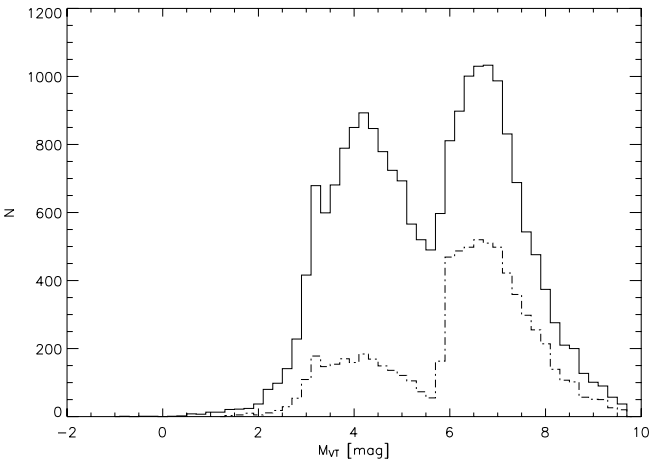

FIG. 2.—Distribution of absolute magnitudes of all DR1 RAVE stars (*solid line*) and our selected sample (*dash-dotted line*). A large fraction have $M_{V_T} > 6$.

of 500 pc and search for overdensities in phase space using the projection technique of Arifyanto & Fuchs (2006). Even the first data release sample is so substantial that we can determine signal-to-noise ratios for orbital "overdensities" and show the statistical significance of the detected overdensities.

2. DATA

The RAVE DR1 (Steinmetz et al. 2006) contains 25,274 radial velocities for 24,748 individual stars, together with proper motions and photometry from other major catalogs (Starnet 2.0, Tycho-2, SuperCOSMOS, USNO-B, DENIS, and 2MASS). Its total sky coverage is $\sim$4760 deg^2. The only missing parameter to obtain all the velocity and position components is a distance estimate. The photometric data, however, allow the application of a photometric parallax relation.[3] To calibrate such a relation for RAVE stars, we used main-sequence (MS) stars (luminosity class V) from the *Hipparcos* Catalogue (ESA 1997) with accurately known parallaxes ($\sigma_\pi/\pi < 0.1$) that could also be identified in the Tycho-2, USNO-B, and 2MASS data. These other catalogs contain V_T-, B1-, and H-band magnitudes, respectively.[4]

The absolute magnitudes of the stars were calculated according to

$$M = m - 10 + 5 \log \left(\frac{\pi}{1 \text{ mas}} \right). \quad (1)$$

We then considered two color-magnitude relations: V_T-H versus M_{V_T} and B1$-H$ versus M_{B1}. Figure 1 shows M_{V_T} versus V_T-H. The dash-dotted line was chosen to remove all stars that seemed to be misclassified as MS stars in the *Hipparcos* Catalogue. This cut was done by eye, since one could only reliably distinguish a (sub-) giant from an MS star in the vicinity of the MS by measuring its surface gravity. Next, the color-magnitude diagram was divided into three color bins in which we separately fitted a color-magnitude relation (*dashed lines*). For each bin, the intrinsic scatter of the color-magnitude relation was calculated as half of the central 68% of the cumulative distribution of the differences ΔM between the true absolute magnitudes (obtained through the parallax) and those obtained through the fit. The scatter in each bin is labeled in Figure 1.

For our analysis we adopted the M_{V_T} versus V_T-H relation, because its intrinsic scatter is slightly smaller than that of M_{B1} versus B1$-H$. Also, the errors on B1 for each star in the RAVE catalog are unknown, while the errors in V_T are given. The formal error in H (from 2MASS) is typically very small, $\sim$0.01 mag. For that reason, we chose the M_{V_T}-(V_T-H) relation to calculate absolute magnitudes M_{V_T} for the RAVE stars. If V_T was not given for a RAVE star, it was possible in most cases to obtain this magnitude through conversion formulae from other magnitudes such as the USNO-B B1 and R1 (R. Klement 2008, in preparation). Figure 2 shows that a large fraction of all DR1 stars have absolute magnitudes fainter than $M_{V_T} = 6$, that is, lie in the section of the color-magnitude relation where its intrinsic scatter is smallest. Therefore, we expect to obtain a large sample of stars with distance estimates good to 10%–20% in most cases (see below and Fig. 2, where the M_{V_T} distribution of our final sample is shown).

We established a right-handed Cartesian coordinate system (x, y, z) centered on the local standard of rest (LSR) with the x-axis pointing in the direction of the Galactic center, the y-axis pointing in the direction of Galactic rotation, and the z-axis in the direction of the north Galactic pole. The quantities U, V, and W denote the velocity components of a star in this Cartesian coordinate system. The Sun is assumed to lie at a distance $R_\odot = 8$ kpc from the Galactic center and to move with velocity $(U_\odot, V_\odot, W_\odot) = (10.0, 5.2, 7.2)$ km s^{-1} with respect to the LSR (Dehnen & Binney 1998). A star's distance d follows from the apparent and absolute magnitudes (V_T, M_{V_T}) via equation (1), with its error σ_d determined through

$$\sigma_d = \frac{d}{5} \ln 10 \sqrt{(\sigma_{V_T})^2 + (\sigma_{M_{V_T}})^2}, \quad (2)$$

where σ_{V_T} and $\sigma_{M_{V_T}}$ denote the errors on V_T and M_{V_T}, respectively. The main error is introduced by the intrinsic scatter of the color-magnitude relation (Fig. 1), which translates into $\sigma_{M_{V_T}}$.

The velocity components of a star can now be calculated from its position, radial velocity v_{rad}, and proper motions (μ_α, μ_δ) through

[3] We assume that the vast majority of RAVE stars are main-sequence stars, because giants in the RAVE magnitude range would lie so far away that the star density is substantially decreased. See also the discussion in Siegel et al. (2002).

[4] We do not consider very metal-poor (sub-) dwarfs, which can lie up to $\gtrsim$1 mag below the solar-metallicity MS; for metal-poor stars we would overestimate the distance and hence velocity. The effect for disk stars, however, will be negligible, because they exhibit approximately solar metallicity. We will come back to the subdwarf problem later in the context of the detection of a new halo stream in the RAVE data.

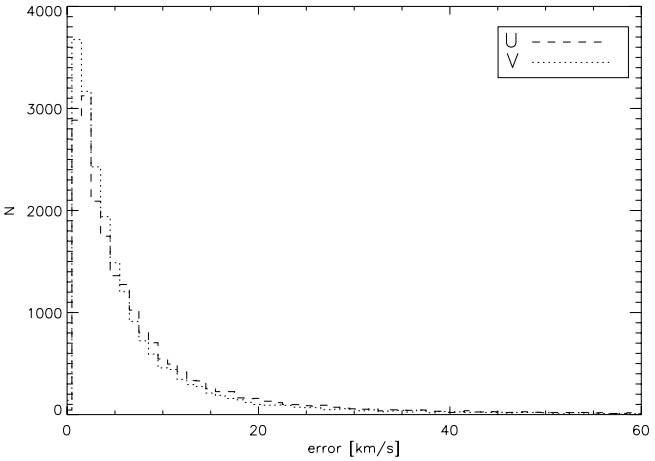

FIG. 3.—Distribution of errors for the velocity components U (*dashed line*) and V (*dotted line*) for all stars in RAVE DR1 as derived from eq. (4). These errors include radial velocity errors, proper-motion errors, and distance uncertainties. Both distributions have a peak around 2–3 km s^{-1} and a long tail reaching to much higher values.

formulae given, for example, in § 3 of Johnson & Soderblom (1987):

$$\begin{pmatrix} U \\ V \\ W \end{pmatrix} = \begin{pmatrix} U_\odot \\ V_\odot \\ W_\odot \end{pmatrix} + \mathbf{B} \begin{pmatrix} v_{\rm rad} \\ 4.74\mu_\alpha d \\ 4.74\mu_\delta d \end{pmatrix}. \quad (3)$$

If μ_α and μ_δ are taken in units of milliarcseconds per year and d in kiloparsecs, the factor of 4.74 gives the result in kilometers per second. The coordinate transformation matrix **B** is defined by Johnson & Soderblom (1987), and we evaluated it for the epoch 2000. The uncertainties in the velocity components depend on the uncertainties in radial velocity, proper motions, and distance:

$$\begin{pmatrix} \sigma_U^2 \\ \sigma_V^2 \\ \sigma_W^2 \end{pmatrix} = \mathbf{C} \begin{pmatrix} \sigma_{v_{\rm rad}}^2 \\ (4.74d)^2[\sigma_{\mu_\alpha}^2 + (\mu_\alpha \sigma_d/d)^2] \\ (4.74d)^2[\sigma_{\mu_\delta}^2 + (\mu_\delta \sigma_d/d)^2] \end{pmatrix} + 2\mu_\alpha\mu_\delta(4.74\sigma_d)^2 \begin{pmatrix} b_{12}b_{13} \\ b_{22}b_{23} \\ b_{32}b_{33} \end{pmatrix} \quad (4)$$

(Johnson & Soderblom 1987). The elements of the matrix **C** are the squares of the corresponding elements of matrix **B**, that is, $c_{ij} = b_{ij}^2$ for all (i, j). About 80% of the stars in the DR1 have radial velocity accuracies better than 3.4 km s^{-1}, and 69.1% have a mean proper-motion error of at most 2.6 mas yr^{-1} (Steinmetz et al. 2006). If we restrict our sample to stars within $d_{\rm max} = 500$ pc from the Sun, that is, within a volume $V_{\rm max} = 4\pi d_{\rm max}^3/3$, we can assume a typical distance for a star as the distance where the volume is half as large: $\langle d \rangle = 0.5^{1/3} d_{\rm max} \approx 400$ pc. If we further restrict the sample to stars with relative distance errors $\sigma_d/d \leq 0.25$ and assume a typical proper motion of 15 mas yr^{-1}, we get as an estimate for the uncertainty of the transverse velocity $\lesssim$8.6 km s^{-1}. The velocity error distribution in U and V is shown in Figure 3. It peaks at errors smaller than 5 km s^{-1}.

For the kinematic stream search, we selected only those stars that satisfy the following criteria: $\sigma_d/d \leq 0.25$, $d \leq 500$ pc, a total space velocity $|\boldsymbol{v}_{\rm tot}| \leq 350$ km s^{-1}, and $(\sigma_U, \sigma_V) \leq 35$ km s^{-1}. We also restricted ourselves to stars at $l > 200^\circ$ and $b > 20^\circ$, because in this field the observation density was highest. This leaves 7015 stars, among which we searched for signatures of local stellar streams.

3. SEARCH STRATEGY FOR STREAMS

The distribution of stellar streams in velocity space is not trivial and depends on the origin and the age, or type, of the stream stars (Dehnen 1998; Famaey et al. 2005). Principally, one has to distinguish between two types of streams: dynamical streams, that is, groups of stars that are trapped in a small region of phase space by dynamical resonances, and tidal streams, in which the stars originated from the same bound object, such as a cluster or a satellite galaxy. Once those stars become unbound, they will have slightly different orbits and, hence, frequencies, so that they will phase-mix. This leads to a broadening in the velocity distribution, which is more prominent in the W-component because the vertical frequency is shorter than the horizontal frequencies. These streams will show a typical "banana"-shaped distribution in U and V and a symmetric distribution in U and W (Helmi et al. 2006). The distribution in V of nearby stream stars with similar angular momenta is narrow, because these stars have basically the same azimuth. On the other hand, dynamical streams show a more clumplike structure in U and V. Their location is primarily set by the tangential velocity component V, because V is a measure for the guiding radius of a star in the solar neighborhood, which itself is a measure for the location of Lindblad resonances with a periodic perturbation (Binney & Tremaine 1987; Quillen & Minchev 2005). They also show a broad range of W-velocities due to phase-mixing (Dehnen 1998). Generally, scattering processes and measurement errors tend to symmetrize and broaden the velocity distribution of stellar streams of both types and make it difficult to identify them in velocity space, particularly if the stream is very spread out spatially and consists only of a small fraction of stars compared with the smooth background.

According to Helmi et al. (1999) and Helmi & de Zeeuw (2000), a better approach to searching for streams is in the space spanned by the integrals of the motion—that is, the energy E and angular momentum L_z, $L_\perp = (L_x^2 + L_y^2)^{1/2}$, or $L_{\rm total}$. For example, Helmi et al. (1999) detected two fossil streams originating from the same progenitor as a clump of solar neighborhood halo stars in $(L_z, L_\perp)$-space. Using cosmological N-body simulations, Choi et al. (2007) showed that over 8 Gyr, the overall position of a disrupting satellite and its tidal tails basically remains the same in (E, L_z)-space, but the shape of the distribution shifts and one satellite can produce several apparently disassociated clumps. This, together with the fact that the total angular momentum is not really an integral of the motion, can obscure the signature of a well-defined moving group in phase space. Therefore, Helmi et al. (2006) proposed looking for stellar streams in a space spanned by the apocenter, pericenter, and angular momentum L_z. Moving groups then cluster around lines of constant eccentricity.

We follow a similar approach, in the sense that we try to find stars with the same orbital eccentricity. Our strategy for finding nearby stellar streams in velocity space is based on the Keplerian approximation for orbits, developed by Dekker (1976) and summarized by Arifyanto & Fuchs (2006). We assume an axisymmetric potential and that stars in the same stellar stream move on orbits that stay close together, which is justified by numerical simulations of satellite disruption (Helmi et al. 2006). These stars should form a clump in the projection of velocity space spanned by $(U^2 + 2V^2)^{1/2}$ and V. The latter is related to the angular momentum L_z, which defines the guiding-center orbits of the stars. The

first quantity is a measure of a star's eccentricity e. For a flat rotation curve, e is given by

$$e = \sqrt{\frac{U^2 + 2V^2}{2V_{\rm LSR}^2}}. \quad (5)$$

Here $V_{\rm LSR}$ denotes the circular velocity of the local standard of rest, for which we take the IAU standard value 220 km s^{-1}.

Also, it can be shown that the radial action integral J_R in the Keplerian approximation is approximately equal to $(\frac{1}{2}\pi R_\odot / V_{\rm LSR}) \times (U^2 + 2V^2)$ (B. Fuchs 2007, private communication). Therefore, the quantity $(U^2 + 2V^2)^{1/2}$ should be robust against slow changes in the potential.

For the current investigation, we do not include W-velocity components in our search for local streams because—as mentioned above—strong phase-mixing will smear out any coherent features over short timescales. However, in § 5 we will make use of the W-velocities when we compare our method with the more traditional searches in (U, V, W)- and (L_z, $L_\perp$)-space.

4. RESULTS AND DISCUSSION

We now use the distribution of the 7015 selected RAVE stars in $(U^2 + 2V^2)^{1/2}$ versus V, shown in Figure 4, to search for substructure in the kinematic distribution. Figure 4 also shows the error ellipses for some points; most of the relative errors are rather small, and even though some of the larger errors produce an uncertainty in the exact position of the data points and tend to smear out substructure, several suggestive "overdensities" of stars are visible by eye. In this section we focus on identifying overdensities and on quantifying their significance.

4.1. *The Wavelet Transform*

To this end, we follow the same procedure outlined by Arifyanto & Fuchs (2006) and use the wavelet-transform technique using a two-dimensional analyzing wavelet $\Psi(x, y)$. We bin the data in pixels of 2 km s^{-1} width on each side and calculate the value of the wavelet transform in each bin through

$$\begin{aligned} w(x,y) &= \iint dx'\, dy'\, \Psi(x - x', y - y') \sum_{i=0}^{N-1} \delta(x' - x_i)\delta(y' - y_i) \\ &= \sum_{i=0}^{N-1} \Psi(x - x_i, y - y_i), \end{aligned} \quad (6)$$

where $N = 7015$ is the number of stars in our sample.

Motivated by the work of Skuljan et al. (1999), Arifyanto & Fuchs (2006) used a Mexican-hat–shaped kernel function to detect overdensities in $(U^2 + 2V^2)^{1/2}$ versus V. However, since the former quantity is not uncorrelated with the latter, we expect clumps that would be roughly spherical in, for example, U versus V, to be elongated along $U = 0$. This means that the performance of a Mexican-hat kernel is suboptimal and might influence the significance of the overdensities. Therefore, we build a kernel function that is elongated about a factor q along the V-shaped $U = 0$ lines, in the following way.

We rotate the coordinate axes such that the new V-axis, V', lies along the line $U = 0$ and the new $(U^2 + 2V^2)^{1/2}$ axis is perpendicular to V'. For simplicity, we rename V as x and $(U^2 + 2V^2)^{1/2}$ as y. This implies two different rotations, depending whether the features are elongated in the region $V \le 0$ [clockwise rotation by an angle $\varphi = \arccos(1/\sqrt{3})$] or in the region $V > 0$ (counterclockwise rotation by φ). Based on the Mexican-hat–shaped function, we then express the analyzing wavelet as a function of the new coordinates (x', y') and elongate it along the x'-axis by a factor q:

$$\Psi(x', y') = \left[2 - \frac{x'^2}{(qa)^2} - \frac{y'^2}{a^2}\right] \exp\left[-\frac{x'^2}{2(qa)^2} - \frac{y'^2}{2a^2}\right]. \quad (7)$$

This function is normalized in the sense that its volume integral is zero. The scale parameter a is a measure for the extent of the "bumps." With the transformation equations

$$x' = \sqrt{\tfrac{1}{3}}x \mp \sqrt{\tfrac{2}{3}}y, \quad y' = \pm\sqrt{\tfrac{2}{3}}x + \sqrt{\tfrac{1}{3}}y, \quad (8)$$

where the upper signs stand for the case $V \le 0$, it is straightforward to calculate the kernel in the unrotated coordinate system:

$$\begin{aligned} \Psi(x,y) = \Bigg\{ 2 - \frac{1}{3(qa)^2}\big[(1 + 2q^2)x^2 + (2 + q^2)y^2 \\ \mp (1 - q^2)2\sqrt{2}xy\big] \Bigg\} \\ \times \exp\Bigg\{ -\frac{1}{6(qa)^2}\big[(1 + 2q^2)x^2 + (2 + q^2)y^2 \\ \mp (1 - q^2)2\sqrt{2}xy\big] \Bigg\}. \end{aligned} \quad (9)$$

Then equation (6) can be used to calculate the value of the wavelet transform in each bin.

For the elongation parameter q, we used $\sqrt{3}$ because the projection of a given range in V along the line $U = 0$ is $\sqrt{3}$ times as long. For the scale parameter a we chose 7 km s^{-1}, comparable to the mean errors, which extracts the overdensities most clearly (Fig. 5).[5]

Figure 5 shows that the bulk of our sample stars have thin-disk–like kinematics, with $|U|$- and $|V|$-values $\lesssim$20 km s^{-1}. The contour levels do not reflect some finer structures at -80 km s$^{-1} \lesssim V \lesssim 20$ km s^{-1}. In this range we would expect the Hercules stream ($V \approx -50$ km s^{-1}), as well as the Hyades-Pleiades ($V \approx -20$ km s^{-1}) and Sirius-UMa ($V \approx +4$ km s^{-1}) streams (Famaey

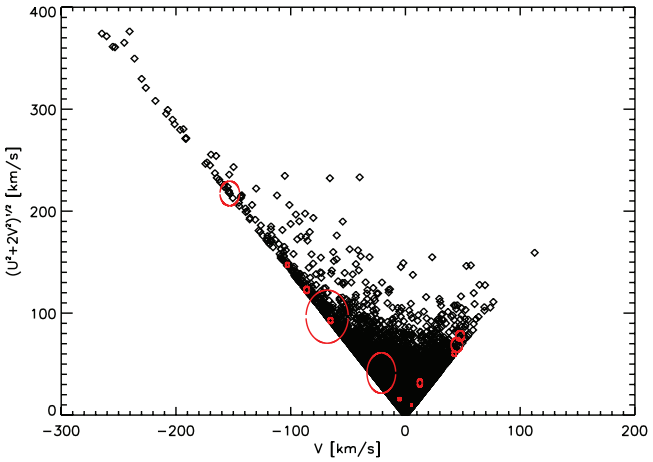

FIG. 4.—Distribution of our sample of RAVE stars in $(U^2 + 2V^2)^{1/2}$ vs. V. We also show error ellipses for a small subset of stars; note that while the large error ellipses are most prominent, most ellipses are very small.

[5] We also tested different choices for the set (q, a), such as ($\sqrt{2}$, 8 km s^{-1}), and basically obtained the same results.

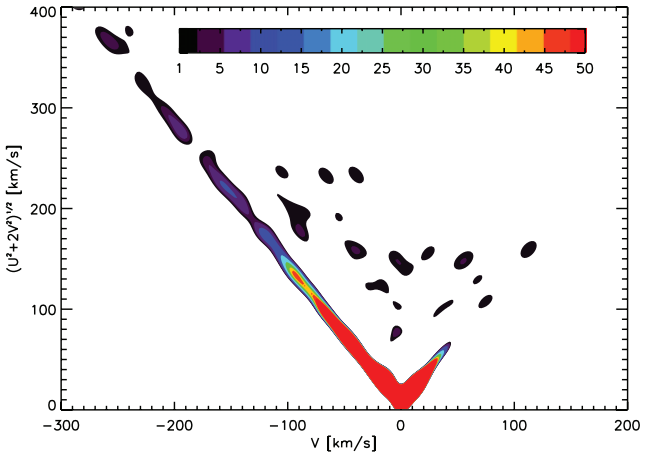

FIG. 5.—Contours of the wavelet transform of the distribution of our sample of RAVE stars (eq. [6]) in $(U^2 + 2V^2)^{1/2}$ vs. V. The contour levels are displayed in the color bar; the scale parameter of the analyzing wavelet is 10 km s^{-1}.

et al. 2005). Indeed, the distribution in $((U^2 + 2V^2)^{1/2}, V)$ is somewhat bulged at these velocities.

Among the stars with high orbital eccentricities, presumably thick-disk or halo stars, Figure 5 appears to show five different overdensities. The first, at $V \approx -95$ km s^{-1}, is most probably the stream that was discovered independently by Arifyanto & Fuchs (2006) and Helmi et al. (2006). The second overdensity, at $V \approx -120$ km s^{-1}, has the same kinematics as the Arcturus group, discovered by Navarro et al. (2004). These two streams most probably have an origin external to the Milky Way disk, because their phase-space distributions resemble that of simulated accreted dwarf satellites (Helmi et al. 2006). However, nothing is known about their progenitors yet. The third feature, at $V \approx -160$ km s^{-1}, has to our knowledge not yet been described in the literature. The same is true for the two clumps at $V \approx -200$ km s^{-1} and $V \approx +50$ km s^{-1}. However, at these velocities our sample is very sparsely populated, so that just a few stars are enough to create a high value of the wavelet transform. Every isolated star in the middle of a bin increases the value of the wavelet in that bin by 2. This also explains the other clumps lying off the V-shaped main feature in Figure 5.

4.2. *Subtracting a Smooth Velocity Distribution*

To test whether any of these kinematic overdensities, or streams, reflected as peaks or clumps in the wavelet transform are significant, we performed 250 Monte Carlo (MC) simulations of the same number of stars as in our sample, which we randomly draw from a Galactic model consisting of three Schwarzschild distributions (Binney & Tremaine 1987) to represent the thin and thick disk and the halo. The goal was to create a "smooth" reference model velocity distribution that matches the overall velocities of the RAVE sample. To this distribution we then added normally distributed velocity errors, based on the observed error distributions shown in Figure 3. We chose local thick-to-thin disk and halo–to–thin-disk normalizations of 0.1 and 0.001, respectively, in agreement with the value from Chen et al. (2001) and Juric et al. (2008) and the upper limit given by Siegel et al. (2002). The thin and thick disk and halo are assumed to have velocity dispersions $(\sigma_U, \sigma_V, \sigma_W)$ and rotational offsets from the LSR equal to (25, 21, 17, −5), (74, 50, 50, −44), and (189, 97, 100, −219) km s^{-1}, respectively. The values for the thin disk were chosen to best match the smooth part of the observed velocity distribution (Fig. 6), although the ratio σ_U/σ_V in the thin disk should be approximately 1.6 (Dehnen & Binney 1998). Also, we chose offsets in the W-distribution of +3 and +10 km s^{-1} for the thin and thick disks to obtain a good match.[6] The matches shown in Figure 6 are not perfect, but the slope of the velocity distribution at negative V-velocities is reproduced well in the simulation. The distributions differ most clearly around $V = 0$, because—possibly as a consequence of the Sirius moving group—the RAVE stars are peaked around $V \approx +5$ km s^{-1}. Moreover, the assumption of a Schwarzschild distribution does not reflect the skewness of the velocity distribution due to the asymmetric-drift effect.

For each MC sample of 7015 stars, we binned the velocities and calculated the wavelet transform in each bin the same way as for the real sample. Figure 7 displays one randomly chosen MC realization. One can clearly detect several peaks in the wavelet transform, seeming "overdensities," which must be, however, by construction, due to Poisson noise. This shows that in our real sample the possibility for such "fake" streams also exists.

[6] This deviation from the expected mean value of $\bar{W} = 0$ could be due to the limited sky coverage of our sample.

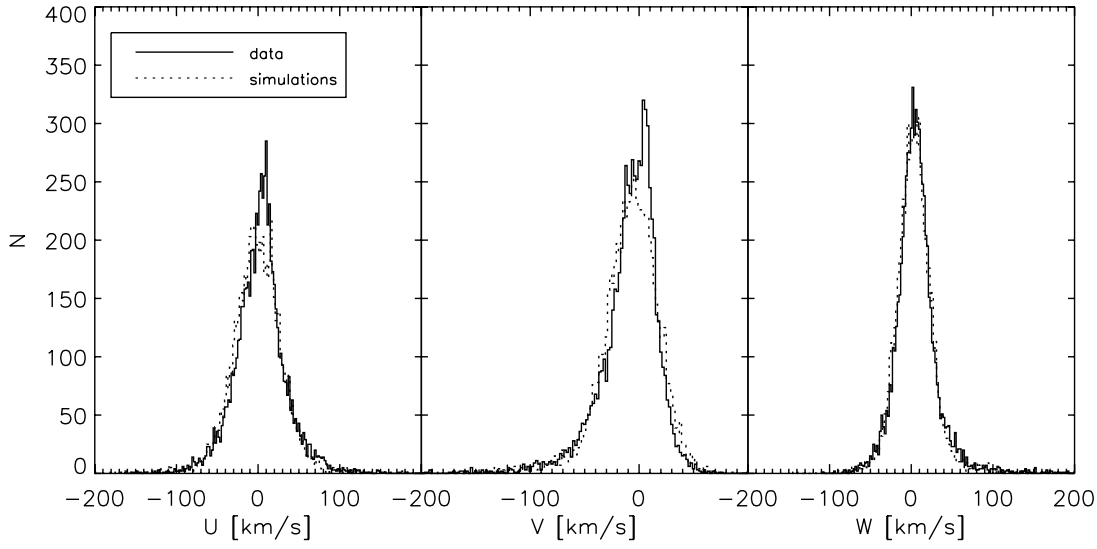

FIG. 6.—Velocity distributions of our selected RAVE stars compared with one MC realization. The MC sample consists of three Schwarzschild distributions for the thin and thick disks and the halo, respectively. Note the peak in the data at around $V = +4$ km s^{-1}, which we interpret as the Sirius moving group below.

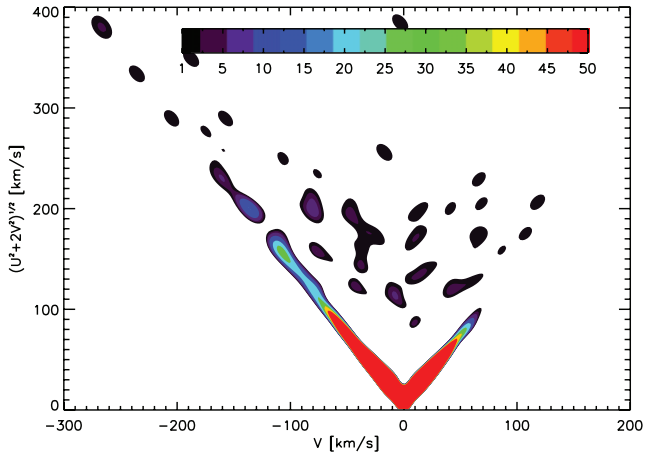

FIG. 7.—Same as Fig. 5, but now for one of our 250 Monte Carlo samples of 7015 stars drawn from a smooth velocity model (§ 4). Because of Poisson noise, some overdensities emerge.

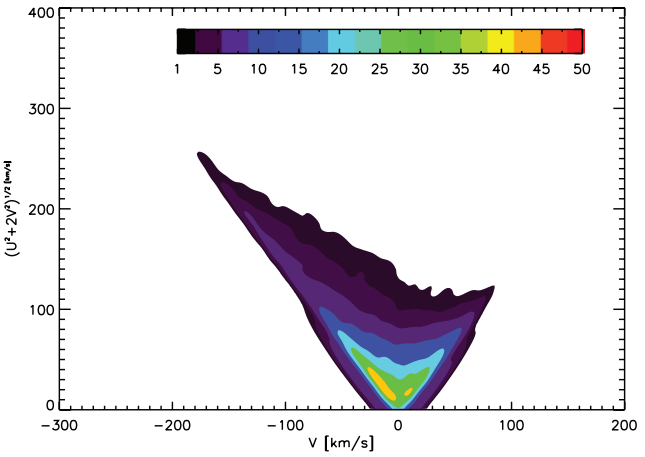

FIG. 9.—Same coordinates as Figs. 7 and 8, but here the standard deviation of the wavelet transform among the 250 Monte Carlo samples is shown. Outside of the contoured region, the variance is set to unity. This variance map is used to asses the significance of wavelet transform peaks in Fig. 5.

We proceeded to calculate the mean value $\bar{w}_{i,j}$ and the standard deviation $\sigma_{i,j}$ of the 250 MC wavelet transforms in each (i, j)-bin. Because many bins are not populated with stars, the standard deviation in those formally has values $\sigma_{l,j} < 1$; when this was the case, we set $\sigma_{l,j} = 1$. The contours of the mean and the standard deviation are shown in Figures 8 and 9, respectively.

While a single Monte Carlo sample shows various kinds of clumps and overdensities due to statistical fluctuations (Fig. 7; see also Arifyanto & Fuchs 2006), the mean value of all wavelet transforms represents a very smooth distribution, because the clumps disappear when averaging over all samples. The standard deviations $\sigma_{l,j}$ define the significance of structure in our real sample in the following way: Because we are only interested in overdense regions, that is, pixels where the wavelet transform takes positive values, we set the value of the wavelet transform of the data, $w^{\rm obs}_{l,j}$, as well as the mean value of the wavelet transform of the 500 MC samples, $\bar{w}^{\rm MC}_{i,j}$, to zero whenever it is ≤ 0. By doing so, we make sure that the residual $w^{\rm obs}_{i,j} - \bar{w}^{\rm MC}_{i,j} \geq 0$ in each pixel, where our "smooth" model contains no stars. By dividing the residual $w^{\rm obs}_{i,j} - \bar{w}^{\rm MC}_{i,j}$ in each pixel by $\sigma_{l,j}$ we define the significance of peaks of $w^{\rm obs}_{l,j}$. For a positive stream detection, we require a significance of at least 2. Figure 10 shows the result.

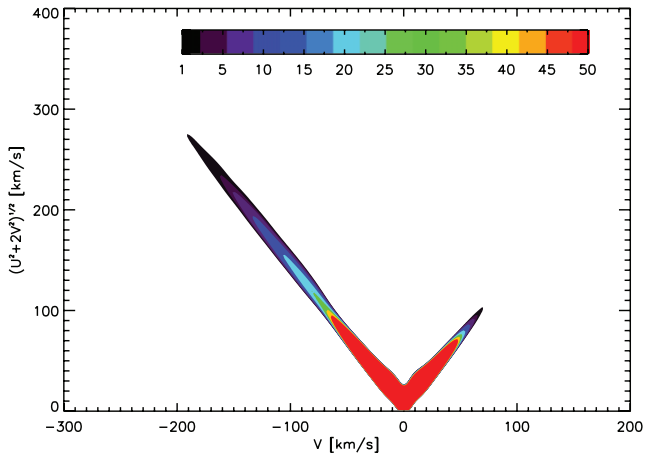

FIG. 8.—Same as Fig. 7, but now the mean value of the wavelet transform for all 250 Monte Carlo samples is shown. Only values ≥1 are displayed.

4.3. *Significance of the Streams*

The first thing to mention is that in all bins where the standard deviation has a value of 1, the significance has the same value as the residual $w^{\rm obs}_{i,j} - \bar{w}^{\rm MC}_{i,j}$. In these bins, one or a few stars will result in a significant overdensity with $\sigma_{l,j} \gtrsim 2$, since for every star in the middle of a bin, the value of $w^{\rm obs}$ increases by 2. This effect could then produce "fake" stellar streams, just because of Poisson noise in our RAVE sample and the smoothness of the combined Monte Carlo samples. Since a solution to this problem is difficult, we avoid speculating about the overdensities in bins with $\sigma_{l,j} = 1$, which we have circled in red in Figure 10. We only give the number of stars that are contained in these features, as derived from the scatter plot (Fig. 4). For example, the extended clump at $V \approx -200$ km s^{-1} corresponds to a group of eight stars, while that at $V \approx -230$ km s^{-1} contains only two. Further investigations with more data could provide more hints toward the nature of these features.

We try to match the remaining statistically significant peaks with streams that have already been described in the literature.

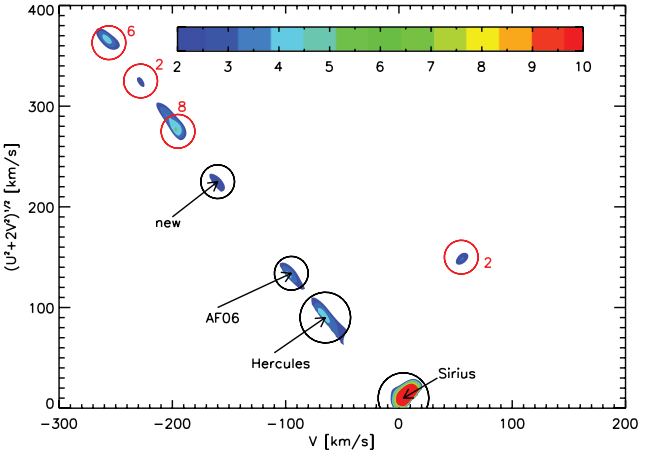

FIG. 10.—Significance of the overdensities seen in Fig. 5, obtained as described in the text. Note that only areas with $\sigma \geq 2$ are displayed. We encircled in black and labeled all features that we consider to be stellar streams. We are not making further suggestions about the four features circled with red but instead give the number of stars that make up these features.

Centered at $V \approx +4$ km s^{-1} and $|U| \approx 10$ km s^{-1} there is a large clump, significant at a level of $\gtrsim$10. This is probably the Sirius-UMa moving group (Dehnen 1998; Famaey et al. 2005), its signal possibly amplified through the inability of our simple three-component MC models to fully match the observed thin-disk distribution (see also Fig. 6). The core of this group is in the direction of Ursa Major. Its members are distributed all around the sky and can be very close (Sirius, at 2.65 pc distance, is a member of the group), putting the Sun inside the group (Bannister & Jameson 2007 and references therein). The current understanding is that the Sirius stream consists not only of a cluster of coeval stars, but also of different kinds of field stars, which altogether could have been forced onto similar orbits by a spiral wave's gravitational field (Sellwood & Binney 2002; Famaey et al. 2005; Quillen & Minchev 2005).

The elongated clump stretching from $V \approx -50$ km s^{-1} to $V \approx -75$ km s^{-1}, with peak significance $\sigma = 4.5$, can probably best be described as the Hercules stream. This stream can be explained by the scattering of stars off the Galactic bar, induced by the outer Lindblad resonance (Dehnen 2000). Famaey et al. (2005) also found a group of, most likely, thick-disk and halo stars located at $V = -53.3 \pm 41.36$ km s^{-1}. Further, at $V = -60$ km s^{-1} there exists the moving group HR 1614, which is thought to be a dispersed open cluster because of its chemical homogeneity (Eggen 1996; De Silva et al. 2007). It is possible that these groups are present in our data, too, amplifying and elongating the signal of the Hercules stream. Better velocity estimates would be needed in order to clearly distinguish between these features.

The feature at $V \approx -100$ km s^{-1} stands out at the 4.3 σ level. It corresponds to the "AF06" stream discovered independently by Arifyanto & Fuchs (2006) and Helmi et al. (2006). Most probably, this stream has its origin outside of the Galaxy and is a relic from the building up of the Milky Way.

At a velocity of $V \approx -160$ km s^{-1}, there is an overdensity that stands out at the 3.0 σ level in the center. A comparison with Figure 5 reveals that this feature is probably more elongated, as one would also expect for a moving group of stars at such velocities. However, with the current sample size our method seems not to be fully able to recover the range from $V = -180$ km s^{-1} to $V = -140$ km s^{-1} as a statistically significant overdensity. Figure 11 shows the stars that make up the new feature in a color-magnitude diagram consisting of $V_T - H$ color and absolute magnitude M_{V_T}. Stars that lie in the area with a significance greater than 2 are plotted with heavy asterisks, while those that lie in the range $V = -180$ km s^{-1} to $V = -140$ km s^{-1} and presumably also belong to the stream have light asterisks. We also show isochrones for a 13 Gyr old population of stars with metallicities [Fe/H] of -1.5, -1.0, and 0.0 (*left to right*). Most of the stars seem to be consistent with having solar metallicity; however, this is a result that would be expected from the way we calculated their distances and velocities. Our assumption was that all are MS stars of luminosity class V, and therefore we a priori excluded the possibility of having very metal-poor (sub-) dwarfs with fainter luminosities (see also footnote 2, in § 2). Right now, we can only wait for future data releases that provide metallicity estimates to solve this issue.

In the Appendix, we investigate the Geneva-Copenhagen Survey of the Solar Neighbourhood (Nordström et al. 2004) with our method; although we do not determine the significance of overdensities with the help of MC sampling, we can see the same strong features detected by Helmi et al. (2006). It is striking that the same stellar streams can be detected in different data sets using different methods.

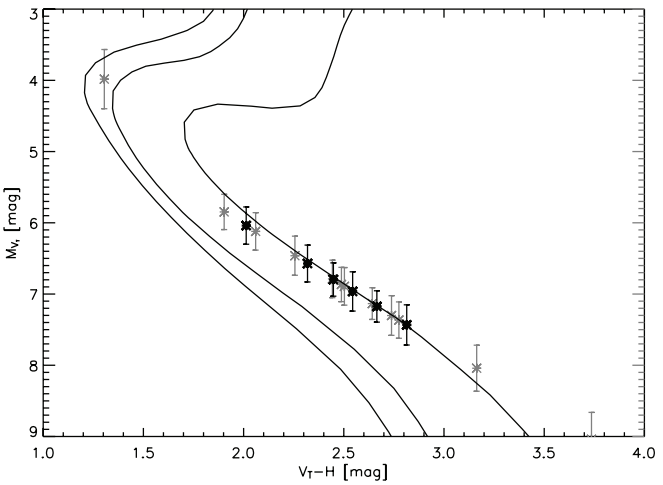

FIG. 11.—Color-magnitude diagram of the stars that make up the feature between $V \approx -140$ km s^{-1} and $V \approx -180$ km s^{-1}, highlighting those in the significantly overdense region -167 km s^{-1} $< V < -153$ km s^{-1} (*heavy asterisks*). Also, isochrones for a 13 Gyr old population with metallicities [Fe/H] of -1.5, -1.0, and 0.0 are plotted. The linearity of our adopted photometric parallax relation in the range $V_T - H > 1.9$ is clearly visible.

Therefore—through the detection of three already known stellar streams in our small RAVE data set—we have enough confidence to claim that the new feature centered on $V = -160$ km s^{-1} is a strong candidate for a new stellar stream. The W-velocities of stars in this feature show a wide range of values, which makes it likely that this stream was accreted long ago as tidal debris during the formation of the Galaxy. To draw more conclusions, one would need metallicity measurements, which will be available from RAVE in the future.

It is possible to place constraints on the density contrast in the streams in the Milky Way stellar halo. Therefore, we estimate how many stars are needed to yield a significant stream detection and divide this number by the total number of halo stars. Because from kinematics alone it is very difficult to delimit halo from thick-disk stars (and even with metallicities there is no clear boundary; see Chiba & Beers 2000), we simply take all stars outside $(V \pm 2\ \sigma_V)_{\text{thin disk}} = -5 \pm 42$ as halo stars and accept a contamination from the thick disk. This gives 554 stars, of which 230 (42%) are part of the Hercules stream, 47 (9%) belong to the AF06 stream, and seven (1%) make up the newly detected stream. We conclude that a few-percent density contrast is enough to provide a significant stream detection.

5. SEARCHING FOR STELLAR STREAMS IN (U, V, W)- AND (L_z, $L_\perp$)-SPACE

The traditional concept of moving groups refers to distinct clumps in (U, V, W) velocity space (Eggen 1996 and references therein). However, as explained in § 3, this space is not immune to the effects of phase-mixing: over time, distinct clumps will disperse as a result of small initial differences in the oscillation periods of the constituent stars and encounters with, for example, molecular clouds. For a part of a stellar stream to be in the solar neighborhood at the same time means that its stars must have similar V-motions, but the U- and W-velocities can differ by hundreds of kilometers per second.

In contrast, stellar streams are able to remain as coherent features in the space of integrals of the motion. Therefore, in the style of Helmi's work (Helmi et al. 1999), we investigate to what extent the detected streams from Figure 10 can be recovered in (U, V, W)- and (L_z, $L_\perp$)-space.

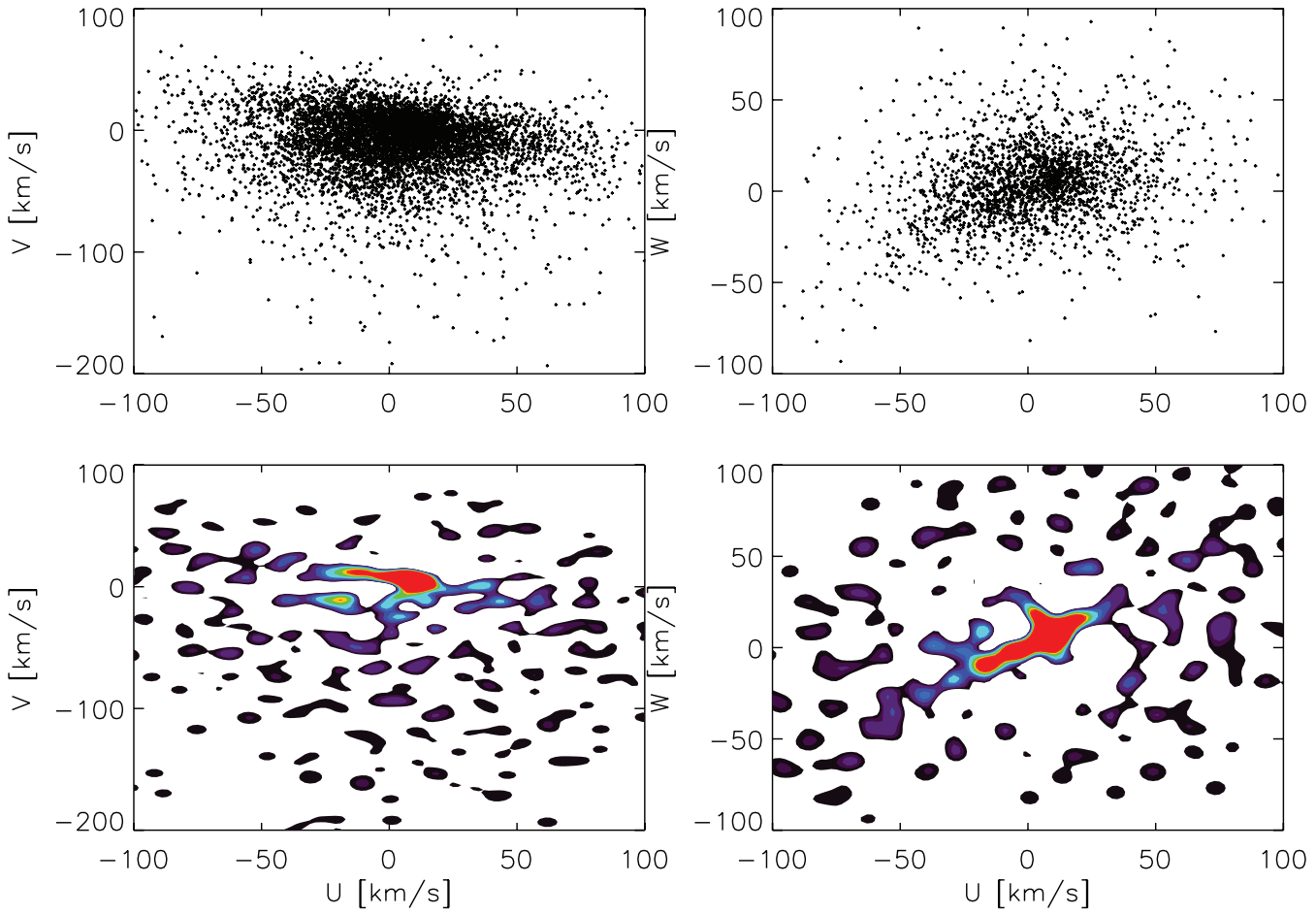

FIG. 12.— Distribution of RAVE stars in velocity space. The top panels show scatter plots of U vs. V and U vs. W, respectively. A great deal of substructure can be seen. In the bottom panels, we show contours of a wavelet transform of the data. The convolution has been made using a Mexican-hat kernel with scale parameter $a = 5$ km s^{-1}.

5.1. *Analyzing the RAVE Data in* (U, V, W)-*Space*

In Figure 12, we show the distribution of our 7015 RAVE stars in velocity space. The top panels show how the stars are distributed with respect to their (U, V, W)-velocities. The distribution is far from smooth, as can be seen more clearly in the bottom panels, where we display the wavelet transform of the velocity components. For the convolution we chose a Mexican-hat kernel with a scale parameter of $a = 5$ km s^{-1} (similar to Skuljan et al. 1999). The contour levels range from 1 (*black*) to 50 (*red*). The most striking features are located around $V = 0$, $U = 0$ and most probably can be attributed to dynamical thin-disk streams such as the Sirius moving group. The elongated shape along the U-axis is typical of stellar steams and is caused by the fact that we observe stars with slightly different orbital phases. The classical moving groups Sirius, at (U, V) $\approx$ (+6, +4) km s^{-1}, the Hyades-Pleiades, at (U, V) $\approx$ (−25, −15) km s^{-1}, and Hercules, at (U, V) $\approx$ (−20, −50) km s^{-1}, can be found with good agreement with the values given by Famaey et al. (2005). The incomplete sky coverage of our sample, as well as the already described effects of phase-mixing, makes it hard to speculate about the meaning of the many other clumps. We nevertheless performed a statistical Monte Carlo analysis analogous to that described in § 4.2 using 200 Monte Carlo simulations. Figure 13 provides the significance map of the velocity space, showing all overdensities from Figure 12 that have a significance of at least 2.

Compared with (V, $(U^2 + 2V^2)^{1/2}$)-space (cf. Fig. 10), there are more features present, but most are very small and at lower

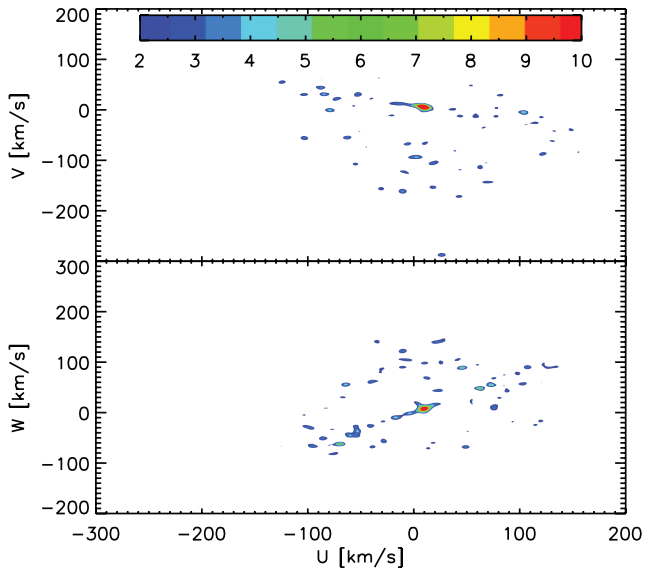

FIG. 13.— Significance of the overdensities seen in Fig. 12. Only areas with $\sigma \geq 2$ are displayed. Note the richness of features compared with Fig. 10, with many having a very small extension.

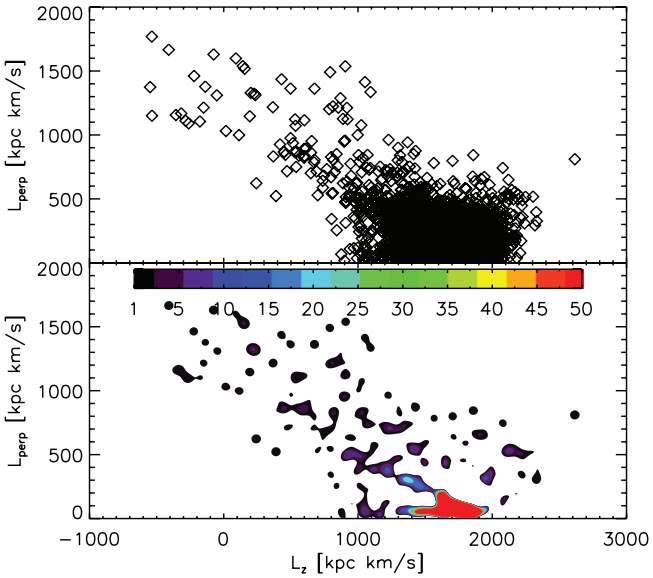

FIG. 14.—Distribution of RAVE stars in $(L_z, L_\perp)$-space. The top panel is a scatter plot of the data. In the bottom panel, we show contours of a wavelet transform of the data. The convolution has been made using a Mexican-hat kernel with scale parameter $a = 45$ km s^{-1}.

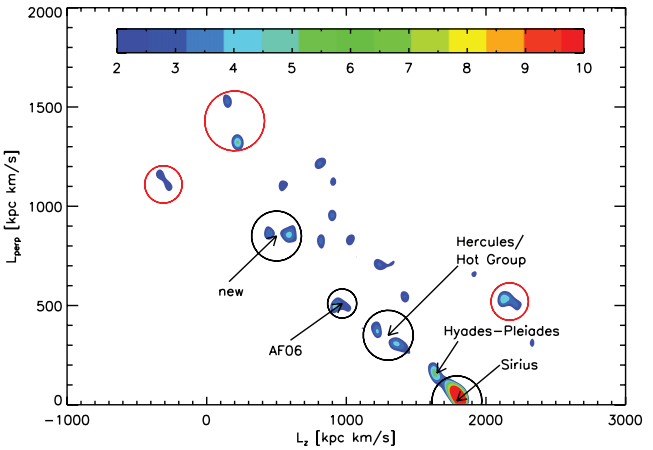

FIG. 15.—Significance of the overdensities seen in Fig. 14. Only areas with $\sigma \geq 2$ are displayed. Black circles mark features that we connect to the detections of Fig. 10; there is further evidence for the now significant Hyades-Pleiades group. Red circles mark features that can be connected to doubtful features in Fig. 10. Note that for stars near the Sun $L_z \approx R_\odot V$, where we take $R_\odot = 8$ kpc.

significance levels. Besides the prominent red feature around $(U, V) \approx (0, 0)$, which can be attributed to the Sirius stream, it is not easy to associate the identified streams from Figure 10 with clumps in the (U, V)- or (U, W)-diagrams. Because old moving groups are not expected to remain coherent as small clumps in velocity space, we have likely overresolved substructure due to the small deviations of our Monte Carlo model from the data. These deviations can also lead to a washing out of the banana-shaped structures in (U, V) that are expected for old tidal streams (Helmi et al. 2006). Large errors in the velocities can wash out these structures, too, but in our case the errors are small enough and should allow their detection. The facts that a clear classification of particularly old stellar streams from the (U, V)- and (U, W)-distributions is not possible and that many small features are even less significant than the overdensities in $(V, (U^2 + 2V^2)^{1/2})$-space lead us to conclude that (U, V, W)-space is not well suited to the detection of moving groups.

5.2. *Analyzing the RAVE Data in* $(L_z, L_\perp)$*-Space*

In a spherical static potential, the two components of the angular momentum, L_z and $L_\perp = (L_x^2 + L_y^2)^{1/2}$, are integrals of the motion. In this case, tidal and dynamical streams remain as coherent clumps in $(L_z, L_\perp)$-space. The assumption of a spherical potential seems valid for large heights above or below the disk that are reached only by halo stars, but not necessarily in our case of nearby stars with planar orbits. These stars move under the influence of a flattened potential, and the radial action integral J_R would be better suited as a conserved quantity. The space of integrals of motion has been shown to be useful for the detection of stellar halo streams in recent studies (Helmi et al. 1999; Helmi & de Zeeuw 2000; Chiba & Beers 2000).

In Figure 14, we show the distribution of our RAVE stars in $(L_z, L_\perp)$-space, again as a scatter plot (*top*) and after wavelet transformation using a Mexican-hat kernel with scale parameter $a = 45$ kpc km s^{-1}. For stars near the Sun, $L_z \simeq R_\odot(V + V_{\rm LSR})$, so we expect to again identify the overdensities from Figure 5.

A comparison shows first of all that $(L_z, L_\perp)$-space seems to be much more structured than $(V, (U^2 + 2V^2)^{1/2})$-space, but this is partly due to the applied chosen scale parameter a in the kernel function. The other reason is that now all three velocity components go into the calculation of the angular momentum components. Also, there are no "forbidden regions" as in the case of $(V, (U^2 + 2V^2)^{1/2})$-space.

Some overdense regions in the bottom panel can be related to overdensities in $(V, (U^2 + 2V^2)^{1/2})$-space. For example, the "bump" in the distribution in Figure 5 at $V \approx -15$ km s^{-1} is also present in Figure 14 at $L_z \approx 1640$ kpc km s^{-1}. Also, the Hercules stream is present at $L_z \approx 1350$ kpc km s^{-1}.

We proceeded to investigate which overdensities prove significant in the same way as before, by using 200 MC samples that were drawn from the three-component Galaxy model described in § 4.2. After building the mean value and standard deviation of their wavelet transforms we derived the significance map, which is shown in Figure 15.

As in the case of (U, V, W)-space, the number of features with significance $\sigma \geq 2$ is larger than in Figure 10. We think that this is caused by the extra information of the W-velocity required for the MC samples. Some of these features are very small and again belong to regions of phase space that are sparsely sampled, but others seem to be comparable to the already known ones. We circled all features that correspond to the detections of Figure 10 with black for the appointed streams and with red for the doubtful ones. In addition, there is a new feature present at $L_z \approx 1650$ kpc km s^{-1}, which we identify as the Hyades-Pleiades group. A hint to the presence of this group has already been seen as a "bulge" in the distribution of stars in $(V, (U^2 + 2V^2)^{1/2})$-space (Fig. 5). It is interesting that some distinct features in $(L_z, L_\perp)$-space (e.g., the new stream) project onto the same feature in $(V, (U^2 + 2V^2)^{1/2})$-space. Furthermore, when we select stars from the fastest-rotating clumps (Hyades-Pleiades, Sirius, and the red-encircled clump on the right in Fig. 15), we find that they span a wide range of values in $(U^2 + 2V^2)^{1/2}$. On the other hand, we also find that clumps in $(V, (U^2 + 2V^2)^{1/2})$-space are not necessarily projected onto clumps in $(L_z, L_\perp)$-space, indicating that $L_\perp$ is not conserved for their motion. Therefore, we conclude that $L_\perp$, compared with $(U^2 + 2V^2)^{1/2}$, is not a good choice as an approximate integral of the motion if the disk's potential dominates the movement of the stars.

We note as a main result that the significances of the detected features are comparable, no matter which space we use for the

stream search. As explained above, we expect the significance of the detections to go up with a larger sample size. For best results, it would probably be good to combine searches in (L_z, $L_\perp$)- and (V, $(U^2 + 2V^2)^{1/2}$)-space to find stellar streams on both inclined and planar orbits. Also, the significance is influenced by the statistical method used to identify overdense regions. Our MC method has the drawback that a good Galactic velocity distribution model is needed in order to avoid "fake" detections in regions where data points are scarce. A combination of different analyses might also enhance the detection efficiency.

6. CONCLUSIONS

To explore RAVE's practical potential for finding kinematic substructures (streams, or moving groups) in the solar neighborhood, we have studied a sample of 7015 nearby stars from the first RAVE public data release, which was selected to have acceptable distance and velocity estimates. Distances were derived from a photometric parallax relation, based on *Hipparcos* main-sequence stars using the V_T and H bands. For our sample, we required a distance error better than 25%, while the mean velocity errors in U and V are approximately -5 km s^{-1}, respectively.

To search for streams, we plotted V-velocities against the quantity $(U^2 + 2V^2)^{1/2}$, which essentially corresponds to angular momentum L_z versus orbital eccentricity e. Streams should form clumps in this projection of phase space. To make such clumps more identifiable, we applied a wavelet transform with a modified two-dimensional Mexican-hat kernel as the analyzing wavelet. Several overdensities are visible in this sample, presumably corresponding to stellar streams. We tested whether these clumps are real or due to Poisson noise using 250 Monte Carlo simulations drawn from a three-component Schwarzschild distribution. While it is very difficult to draw conclusions about the amount and significance of substructure present in the very few halo stars, we did detect three already known stellar streams and one candidate for a newly discovered stream. The latter is present as a broad feature in the range -180 km s^{-1} $\leq V \leq -140$ km s^{-1} centered at $V \approx -160$ km s^{-1} and, from its kinematics, would belong to the stellar halo population. Its other velocity components (high W-velocities, with mean $\bar{W} = 117 \pm 26$ km s^{-1}, $\bar{U} = 6.7 \pm 55$ km s^{-1}) make it likely that this stream is part of the tidal debris from an accreted satellite rather than being due to a dynamical resonance. The kinematics, however, could be somewhat biased, because we did not correct for metallicity effects in the photometric parallax relation. The other moving groups are the Sirius stream, at $V \approx +4$ km s^{-1}, the Hercules stream, centered at $V \approx -65$ km s^{-1} (Dehnen 1998; Famaey et al. 2005), and the stream discovered by Arifyanto & Fuchs (2006) and Helmi et al. (2006) at $V \approx -100$ km s^{-1}.

We are missing a detection of the Hyades-Pleiades and Arcturus streams, which were still present as peaks in the wavelet transform of the data in Figure 5. Here the difference $w^{\rm obs}_{i,j} - \bar{w}^{\rm MC}_{i,j}$ is too small to make the peak in $w^{\rm obs}_{l,j}$ statistically significant.

However, we were able to detect the Hyades-Pleiades moving group in velocity and angular momentum space, which we used to complement our stream search. By comparing the detections in (U, V, W)-, (L_z, $L_\perp$)-, and (V, $(U^2 + 2V^2)^{1/2}$)-space, we showed (1) that the significances of the features are comparable, (2) that velocity space is suboptimal for detecting stellar streams but may be useful for additional information on the age and origin of a stream (tidal streams look different from dynamical streams, old streams disperse), and (3) that $L_\perp$ is a poor approximate integral of the motion compared with $(U^2 + 2V^2)^{1/2}$ if the stars are mainly moving under the influence of the disk's potential.

The fact that only a fraction of the RAVE DR1 stars were enough to find significant substructure in the solar neighborhood shows the power of the method used. Subsequent data releases will not only enlarge the sample of stars and eventually allow the detection of further clumps in phase space but will also provide measurements of log g, $T_{\rm eff}$, and [M/H]. The full data set will include these measurements for up to 1 million stars (Steinmetz et al. 2006). Simply speaking, and neglecting an increase in spatial coverage, an enlargement of the sample size by a factor of N leads to N times more stars in a stellar stream, while the standard deviation of the MC samples with be increased by a factor of $\sqrt{N}$ (Poisson noise). The mean value of the wavelet transform of the MC samples stays the same, so that the significance of the features will be $N/\sqrt{N} = \sqrt{N}$ times as high. In this way we can hope to detect more features and place further constraints on the exact nature and origin of the detected streams.

APPENDIX

STREAMS IN THE GENEVA-COPENHAGEN SURVEY

Here we demonstrate the performance of our method with the data taken from the Geneva-Copenhagen Survey of the Solar Neighbourhood (Nordström et al. 2004). Helmi et al. (2006) searched for stellar steams in velocity and apocenter–pericenter–angular momentum (APL) space in these data. While the dynamical streams (Sirius, Hyades-Pleiades, and Hercules) can be seen as clumps in velocity space, a detailed statistical analysis of the APL space revealed around 10 further overdensities oriented along two to three segments of constant eccentricity. Helmi et al. (2006) divided the stars in the overdense regions into three groups based on their metallicities. There seems to be a relation between these three groups, the Arcturus stream, and the stream detected by Arifyanto & Fuchs (2006).

In Figure 16, we just show the distribution of the 13,240 Geneva-Copenhagen stars in V versus $(U^2 + 2V^2)^{1/2}$, after convolution with the analyzing wavelet given by equation (7).[7] The most striking features are those that were also found by Helmi et al. (2006). In addition, a comparison with our RAVE sample (Fig. 5) seems to suggest that there is much more substructure present in the Geneva-Copenhagen Survey, although it contains only $\sim$2 times more stars. We find that 10,582 of the 13,240 stars are included in these features with a value of the wavelet transform $w_{l,j} \geq 1$. That accounts for 79.9% of the sample. Our RAVE sample contains 7015 stars, of which 5601, or 79.8%, correspond to regions with $w_{l,j} \geq 1$. So, it seems that the size of the sample is the main reason that in the Geneva-Copenhagen Survey we find more distinct overdensities. Furthermore, if we connect the number of patches above the V-shaped $U = 0$ line (30 in Geneva-Copenhagen, 14 in the RAVE sample) to the number of stars in the sample, we find a similar relation; the larger number of stars increases the probability of finding outliers in less populated regions. Finally, stars in the Geneva-Copenhagen Survey have accurate trigonometric parallaxes from *Hipparcos* with relative errors (σ_π/π) better than 10%, in contrast to the less accurate photometric parallaxes of our RAVE stars. This implies less accurate velocities, which tend to smear out small nearby features in phase space.

[7] Arifyanto & Fuchs (2006) also performed this analysis, but using the presumably not optimal Mexican-hat analyzing wavelet.

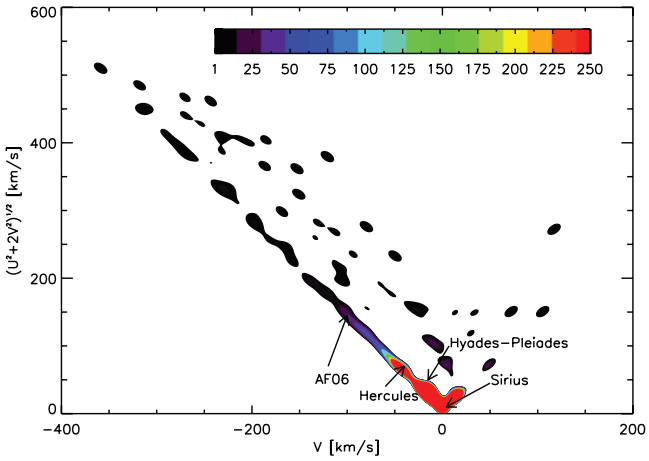

FIG. 16.—Contours of the wavelet transform of 13,440 stars from the Geneva-Copenhagen Survey plotted in V vs. $(U^2 + 2V^2)^{1/2}$ (most of which are not statistically significant). The features described by Helmi et al. (2006) have been labeled.

Although it is unlikely that the majority of the small features in Figure 16 have any statistical significance, this example still shows that a large sample size together with good distance estimates is crucial for detecting stellar streams in phase space. Still, our photometric parallaxes seem to be good enough, and our sample large enough, for significant stream detections. Without investigating the statistical significance of the features in Figure 16, we leave this example as further evidence that stellar streams will be detectable as clumps in $(V, (U^2 + 2V^2)^{1/2})$-space.

REFERENCES

Arifyanto, M. I., & Fuchs, B. 2006, A&A, 449, 533
Bannister, N. P., & Jameson, R. F. 2007, MNRAS, 378, L24
Belokurov, V., et al. 2006, ApJ, 642, L137
Binney, J., & Tremaine, S. 1987, Galactic Dynamics (Princeton: Princeton Univ. Press)
Chen, B., et al. 2001, ApJ, 553, 184
Chiba, M., & Beers, T. C. 2000, AJ, 119, 2843
Choi, J.-W., Weinberg, M. D., & Katz, N. 2007, MNRAS, 381, 987
Dehnen, W. 1998, AJ, 115, 2384
———. 2000, AJ, 119, 800
Dehnen, W., & Binney, J. J. 1998, MNRAS, 298, 387
Dekker, E. 1976, Phys. Rep., 24, 315
De Silva, G. M., Freeman, K. C., Bland-Hawthorn, J., Asplund, M., & Bessell, M. S. 2007, AJ, 133, 694
Eggen, O. J. 1996, AJ, 112, 1595
ESA. 1997, The Hipparcos and Tycho Catalogues (ESA SP-1200) (Noordwijk: ESA)
Famaey, B., Jorissen, A., Luri, X., Mayor, M., Udry, S., Dejonghe, H., & Turon, C. 2005, A&A, 430, 165
Fellhauer, M., et al. 2007, MNRAS, 375, 1171
Helmi, A., & de Zeeuw, P. T. 2000, MNRAS, 319, 657
Helmi, A., Navarro, J. F., Meza, A., Steinmetz, M., & Eke, V. R. 2003, ApJ, 592, L25
Helmi, A., Navarro, J. F., Nordström, B., Holmberg, J., Abadi, M. G., & Steinmetz, M. 2006, MNRAS, 365, 1309
Helmi, A., White, S. D. M., de Zeeuw, P. T., & Zhao, H. 1999, Nature, 402, 53
Ibata, R., Lewis, G. F., Irwin, M., Totten, E., & Quinn, T. 2001, ApJ, 551, 294
Ibata, R. A., Gilmore, G., & Irwin, M. J. 1994, Nature, 370, 194
Ibata, R. A., Irwin, M. J., Lewis, G. F., Ferguson, A. M. N., & Tanvir, N. 2003, MNRAS, 340, L21
Johnson, D. R. H., & Soderblom, D. R. 1987, AJ, 93, 864
Juric, M., et al. 2008, ApJ, 673, 864
Law, D. R., Johnston, K. V., & Majewski, S. R. 2005, ApJ, 619, 807
Majewski, S. R., Skrutskie, M. F., Weinberg, M. D., & Ostheimer, J. C. 2003, ApJ, 599, 1082
Navarro, J. F., Helmi, A., & Freeman, K. C. 2004, ApJ, 601, L43
Nordström, B., et al. 2004, A&A, 418, 989
Peñarrubia, J., et al. 2005, ApJ, 626, 128
Quillen, A. C., & Minchev, I. 2005, AJ, 130, 576
Sellwood, J. A., & Binney, J. J. 2002, MNRAS, 336, 785
Siegel, M. H., Majewski, S. R., Reid, I. N., & Thompson, I. B. 2002, ApJ, 578, 151
Skuljan, J., Hearnshaw, J. B., & Cottrell, P. L. 1999, MNRAS, 308, 731
Steinmetz, M., et al. 2006, AJ, 132, 1645
Yanny, B., et al. 2003, ApJ, 588, 824 (erratum 605, 575 [2004])